

Electronic Supporting Information (ESI)

**Newly Designed 1,2,3-Triazole Functionalized Covalent Triazine Frameworks with Exceptionally High Uptake Capacity of both CO<sub>2</sub> and H<sub>2</sub>**

Soumya Mukherjee,<sup>ab</sup> Monojit Das,<sup>ab</sup> Anupam Manna,<sup>ab</sup> Rajamani Krishna,<sup>c</sup> and Sanjib Das<sup>\*,ab</sup>

<sup>a</sup>Department of Colloids & Materials Chemistry, CSIR-Institute of Minerals & Materials Technology, Bhubaneswar 751013, Odisha, India. Email: sanjibdas@immt.res.in

<sup>b</sup>Academy of Scientific & Innovative Research (AcSIR), Ghaziabad 201002, India.

<sup>c</sup>Van't Hoff Institute for Molecular Sciences, University of Amsterdam, Science Park 904, 1098 XH Amsterdam, The Netherlands.

Section	Contents	Pages
A	Materials and methods	S2-S3
B	General synthetic procedures	S3-S6
C	FT-IR analysis	S6
D	Solid-state <sup>13</sup> C CP-MAS NMR analysis	S7
E	Powder X-ray Diffraction analysis	S8
F	Elemental analysis	S8
G	XPS Survey scan	S8
H	Pure component isotherms (N <sub>2</sub> and CH <sub>4</sub> ) and isosteric heat of adsorption	S9
I	Henry plot for CO <sub>2</sub> , N <sub>2</sub> , and CH <sub>4</sub>	S9-S10
J	Henry selectivity	S10
K	Fitting of pure component isotherms	S10-S11
L	Isosteric heat of adsorption	S11
M	IAST calculations of adsorption selectivities and uptake capacities	S11-S12
N	Transient breakthrough simulations in fixed bed adsorbers	S12
O	Notation used in breakthrough simulations	S13
P	Supporting tables	S13-S16
Q	Supporting figures	S16-S20
R	Structure, synthesis, and characterization of Model Compounds	S20-S23
S	Gas uptake experiments and textural properties of <i>df</i> -TzCTF700 and TzCTF700	S23-S25
T	Supporting references	S25-S26

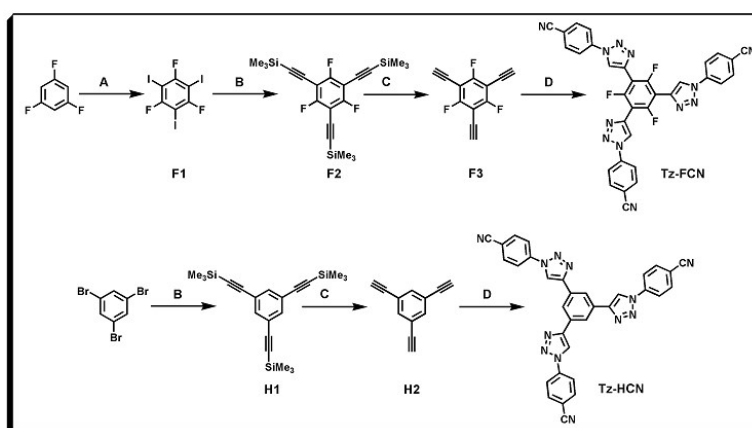
## Section A. Materials and methods:

All chemical reagents were purchased from commercial sources and used as received unless otherwise stated. Periodic acid, dimethylamino pyridine, ammonium formate, potassium iodide, triethylamine,  $\text{CuSO}_4 \cdot 5\text{H}_2\text{O}$ , cesium fluoride, and sodium thiosulfate were purchased from Spectrochem (India). 1,3,5-trifluorobenzene, (trimethylsilyl)acetylene, tetrakis(triphenylphosphine)palladium(0), Pd/C, 5-nitroisophthalic acid, DCC, and sodium ascorbate were purchased from Alfa Aesar. Anhydrous zinc chloride was purchased from Alfa-Aesar and further dried at 110 °C under vacuum prior to use. All organic solvents were procured from Spectrochem (India). Anhydrous THF was prepared by continuously refluxing THF over sodium and freshly distilled under argon. Column chromatography was performed using silica gel purchased from Spectrochem (India).

Solution  $^1\text{H}$ , and  $^{19}\text{F}$  NMR spectra were recorded on a Bruker® Ultrashield instrument operating at a frequency of 400 MHz with tetramethylsilane (TMS) as an internal standard using  $\text{CDCl}_3$  as solvent. All measurements were carried out at ambient temperature and chemical shifts are reported in parts per million (ppm) relative to the deuterated solvent. Solid state cross polarization magic angle spinning (CP-MAS)  $^{13}\text{C}$  NMR was performed at ambient temperature on JEOL JNM-ECX400II solid-state NMR spectrometer operating at a frequency of 400 MHz. Fourier-transform Infrared spectra (FT-IR) of starting materials and as-synthesized TzCTFs were obtained using a Perkin Elmer Spectrum-GX spectrophotometer with KBr pallet in transmittance mode. All FT-IR spectra were background corrected. Powder X-ray diffraction (PXRD) patterns were recorded on a Rigaku Ultima-IV diffractometer using monochromated  $\text{Cu-K}_\alpha$  ( $\lambda = 1.54060 \text{ \AA}$ ) radiation with a scan speed of  $2^\circ \text{ min}^{-1}$  and a step size of  $0.01^\circ$  in  $2\theta$ . The X-ray tube operated at a voltage of 40 kV and a current of 30 mA. Thermogravimetric analyses were carried out in a nitrogen stream using Netzsch STA 449F3-jupiter thermogravimetric-differential scanning calorimetry (TG-DSC) analyzer with a heating rate of  $10^\circ \text{C/min}$ . The Raman spectra were measured on a Horiba LabRAM HR confocal micro-Raman system with excitation source of 532 nm diode-pumped solid state laser. Field emission scanning electron microscopy (FE-SEM) images were taken using Carl Zeiss AG Supra Gemini 55 at an accelerating voltage of 15 kV and equipped with OXFORD energy dispersive X-ray spectrometer. The powder samples were dispersed in ethanol and the suspension was drop casted on a clean piece of silicon wafer. High-resolution Transmission electron microscopy (TEM) images were captured using field-emission JEOL, JEM-2100F at an accelerating voltage of 200 kV. The

powder samples were dispersed in dichloromethane (DCM) and one drop of the suspension was drop casted on a carbon coated copper grid. **Elemental analysis** (C, H, and N) were performed on a Thermo Scientific Flash 2000 Organic Elemental Analyzer. **High resolution X-ray photoelectron spectroscopy (XPS)** spectra were recorded with PHI 5000 Versa Probe II XPS with AES module comprising argon ion as well as C60 sputter guns. All **low pressure gas adsorption-desorption experiments** (up to 1 bar) were carried out on Quantachrome Autosorb-iQ surface area & pore size analyzer. Before gas adsorption experiment sample was degassed first at 140°C under a dynamic vacuum for 12 hours. High-purity-grade He, N<sub>2</sub>, H<sub>2</sub>, CO<sub>2</sub> and CH<sub>4</sub> gases were used in all adsorption measurements. N<sub>2</sub> (77 K) and H<sub>2</sub> (77 K) isotherms were measured using a liquid nitrogen bath. CO<sub>2</sub>, N<sub>2</sub>, and CH<sub>4</sub> isotherms at variable temperatures (from 273 K to 308 K) were measured using a jacketed recirculating dewar containing mixed water and ethylene glycol (1:1 ratio) and the dewar was connected to a chiller (JULABO, FL300, working temperature range: -20 to +40°C, temperature stability: ±0.5°C) having circulating methanol to precisely achieve analysis temperature 308 K, 298 K, and 273 K, respectively. The Brunauer-Emmett-Teller (BET) surface area was calculated over the relative pressure range 0.05 – 0.3 P/P<sub>0</sub> whereas Langmuir surface area calculated taking relative pressure range 0 – 0.15 P/P<sub>0</sub>. Total pore volumes were measured at relative pressure near 0.99 P/P<sub>0</sub> while microporosity was estimated by measuring the pore volume at a relative pressure of 0.1 P/P<sub>0</sub>. Pore size distributions and pore volumes were derived from the isotherms using the non-local density functional theory (NL-DFT) slit pore model on carbon.

## Section B. General Synthetic Procedures:



**A:** HIO<sub>4</sub>·2H<sub>2</sub>O, Conc.H<sub>2</sub>SO<sub>4</sub>, Finely ground KI, 70°C, 6 hours; **B:** Trimethylsilylacetylene, CuI, Pd(PPh<sub>3</sub>)<sub>4</sub>, THF, Triethylamine, 90°C, 12 hrs; **C:** CsF, Ethanol, Tetrahydrofuran, 50 min, RT; **D:** 4-Azidobenzonitrile, Sodium ascorbate, Water, Tetrahydrofuran, 40°C, 3 days.

**Scheme S1:** Synthetic route of Tz-FCN and Tz-HCN building blocks

### Synthetic Procedures:

**1,3,5-trifluoro-2,4,6-triiodobenzene (F1):**<sup>S1</sup> A 100 ml round bottom flask equipped with stir bar was charged with 25 ml conc. H<sub>2</sub>SO<sub>4</sub> and the flask was cooled down to 0°C using an ice-bath. Then HIO<sub>4</sub>·2H<sub>2</sub>O (3.88 g, 17.03 mmol) was added into the mixture over 15 minutes followed by addition of finely grounded KI (8.51 g, 51.27 mmol) in small portions over 10 mins. 1,3,5-trifluorobenzene (1.5 g, 11.3 mmol) was added dropwise via a syringe and the mixture was stirred for 10 minutes while the temperature was held at 0°C. The ice-bath was removed and the reaction mixture was at 70°C for an additional 6 hours. After completion of reaction, the mixture was cooled down to room temperature and poured into crushed ice while stirring. The mixture was extracted with diethyl ether (3 x 50ml) and the combined organic layer was washed by saturated solution of sodium thiosulfate (2x50 ml), water and dried over anhydrous MgSO<sub>4</sub>. The organic layer was evaporated to dryness to afford **F1** as off white colored solid almost quantitatively. The product is directly used in next step without any further purification.

**1,3,5-trifluoro-2,4,6-tris[(trimethylsilyl)ethynyl]benzene (F2):**<sup>S2</sup> A 250 ml two neck round bottom flask equipped with stir bar was charged with 1,3,5-trifluoro-2,4,6-triiodobenzene (1.5 g, 2.94 mmol), CuI (60 mg, 0.294 mmol), and tetrakis(triphenylphosphine)palladium(0) (340 mg, 0.29 mmol), anhydrous THF (40 ml), and freshly distilled triethylamine (40 ml) under argon atmosphere. The reaction mixture was stirred for 30 mins at room temperature followed by dropwise addition of trimethylsilylacetylene (1.21 g, 12 mmol). The mixture was heated at 90°C under inert condition for an additional 12 hours. After completion of reaction, the reaction mixture was cooled down to room temperature, filtered and extracted by dichloromethane (3 x 50 ml). The combined organic layer was washed with water and dried over anhydrous MgSO<sub>4</sub>. The organic layer was evaporated to dryness under reduced pressure. The crude product was purified by silica gel column chromatography (hexane) yielding 1,3,5-trifluoro-2,4,6-tris[(trimethylsilyl)ethynyl]benzene (**F2**) (915 mg, 85 %) as white colored solid. <sup>1</sup>H NMR (400 MHz; CDCl<sub>3</sub>): 0.26 (s, 27H).

**1,3,5-triethynyl-2,4,6-trifluorobenzene (F3):**<sup>S3</sup> A 50 ml round bottom flask equipped with stir bar was charged with 1,3,5-trifluoro-2,4,6-tris[(trimethylsilyl)ethynyl]benzene **F2** (915 mg, 2.17 mmol), 14 ml of THF, and 7 ml of ethanol followed by addition of CsF (1.04 g, 6.84 mmol). The reaction mixture was stirred for 50 minutes at RT under inert condition. The solvent was evaporated under reduced pressure and the crude product was purified by silica

gel column chromatography (hexane:dichloromethane 9:1) yielding **F3** (205 mg, 55 %) as white colored solid. <sup>1</sup>H NMR (400 MHz; CDCl<sub>3</sub>): 3.53 (s, 3H).

**Synthesis of Tz-FCN:** A 250 ml round bottom flask equipped with stir bar was charged with 1,3,5-triethynyl-2,4,6-trifluorobenzene (200 mg, 0.98 mmol), 4-azidobenzonitrile (510 mg, 3.39 mmol), THF (75 ml), and water (30 ml). The resulting clear solution was purged with argon over 30 min at room temperature followed by addition of CuSO<sub>4</sub>·5H<sub>2</sub>O (81 mg, 0.31 mmol) and sodium ascorbate (119 mg, 0.60 mmol). The reaction mixture was heated to 40°C and kept stirring for 3 days under inert atmosphere. The bright yellow precipitate was filtered and washed several times with DMSO, Water, Methanol, DCM, and Acetone, respectively, and finally dried in vacuum oven at 70°C resulting **Tz-FCN** (61% yield; Mp 194 °C) as bright yellow colored solid. The titled compound (**Tz-FCN**) is almost insoluble in all common organic solvents. Solid-state <sup>13</sup>C NMR (ppm): 156, 141, 131, 120, 112, 107; IR (KBr pellet, cm<sup>-1</sup>): 2230, 1607, 1515, 1460, 1400, 1236, 1080, 1039, 987, 841, 735, 551.

**1,3,5-tris[2-(trimethylsilyl)ethynyl]benzene (H1):**<sup>S2</sup> A 250 ml two neck round bottom flask equipped with stir bar was charged with 1,3,5-tribromobenzene (6.0 g, 19.05 mmol), CuI (145.12 mg, 0.762 mmol), PPh<sub>3</sub> (999.32 mg, 3.81 mmol), PdCl<sub>2</sub>(PPh<sub>3</sub>)<sub>2</sub> (668.56 mg, 0.95 mmol), anhydrous THF (60 ml), and diisopropyl amine (60 ml). The mixture was purged with argon over 10 mins at room temperature followed by dropwise addition of trimethylsilylacetylene (6.74 g, 19.05 mmol) under inert condition. The reaction mixture was heated to 70°C for overnight and cooled down to room temperature. The mixture was filtered and the filtrate was extracted by chloroform (3 x 50 ml) and washed with water and then dried over anhydrous MgSO<sub>4</sub>. Organic layer was evaporated to dryness and the crude product was purified via column chromatography (silica gel, hexane) to obtain cream colored solid compound (5.3 g, 80%). <sup>1</sup>H NMR (400 MHz; CDCl<sub>3</sub>): 0.23 (s, 27H), 7.49 (s, 3H).

**1,3,5-triethynylbenzene (H2):**<sup>S4</sup> A 100 ml round bottom flask equipped with stir bar was charged with 1,3,5-tris(2-(trimethylsilyl)ethynyl)benzene (2.0 g, 5.45 mmol) and methanol (60 ml) followed by addition of K<sub>2</sub>CO<sub>3</sub> (4.51 g, 32.70). The clear reaction mixture was stirred at room temperature for 6 hours. After completion of reaction, mixture was filtered and solvent was evaporated to dryness. The crude product was purified by column chromatography (silica gel, hexane) to afford the title compound (750 mg, 91.6% yield). <sup>1</sup>H NMR (400 MHz; CDCl<sub>3</sub>): 3.11 (s, 3H), 7.57 (s, 3H).

**Synthesis of Tz-HCN:** The title compound was synthesized adopting the above mentioned procedure for Tz-FCN using 1,3,5-triethynylbenzene (200 mg, 0.9797 mmol) as starting material resulting yellow colored compound (55.4% yield; Mp 174 °C). The titled compound

(Tz-HCN) is almost insoluble in all common organic solvents. Solid-state  $^{13}\text{C}$  NMR (ppm): 146, 139, 131, 121, 111; IR (KBr pellet,  $\text{cm}^{-1}$ ): 2230, 1607, 1515, 1400, 1236, 1039, 987, 840, 551; Anal. Calcd for  $\text{C}_{33}\text{H}_{18}\text{N}_{12}$ : C, 68.03; H, 3.11; N, 28.85. Found: C, 66.79; H, 3.05; N, 29.41.

**Synthesis of 4-azido benzonitrile:**<sup>S5</sup> A 100 ml round bottom flask equipped with stir bar was charged with 4-aminobenzonitrile (1.18 g, 10 mmol), p-toluenesulfonic acid monohydrate (5.16 g, 30 mmol), and acetonitrile (40 ml). The reaction mixture was cooled down to 0-5 $^{\circ}\text{C}$  and stirred for 1 hour. Ice-cold 6.0 ml sodium nitrite (1.38 g, 20 mmol) solution was added dropwise into the reaction mixture and stirring was continued for 30 min and then solid sodium azide (1.04 g, 16 mmol) was added and the mixture was stirred for an addition 1.0 hour at 10 $^{\circ}\text{C}$ . The reaction mixture was then allowed to room temperature followed by extraction with chloroform (3x25 ml). The chloroform layer was washed by water (3x100 ml) followed by drying the organic part over anhydrous  $\text{MgSO}_4$ . The organic layer was evaporated to dryness under reduced pressure using rotary evaporator. The crude product was purified by column chromatography (silica gel, chloroform: hexane = 3:2) to obtain the title compound (1.01 g, 82%).  $^1\text{H}$  NMR (400 MHz;  $\text{DMSO-d}_6$ ): 7.25 (d, 2H), 7.78 (d, 2H).

### Section C. FT-IR Spectroscopy:

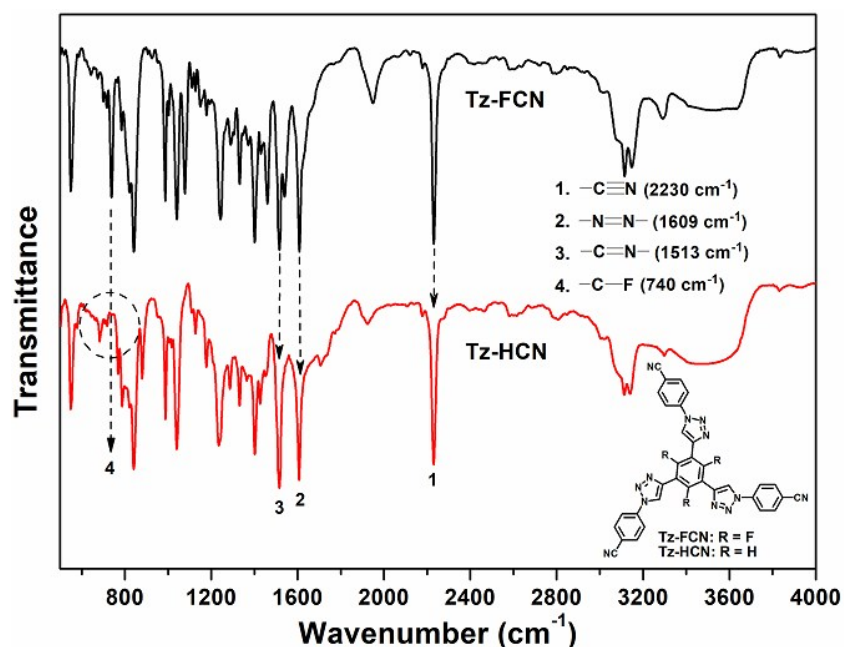
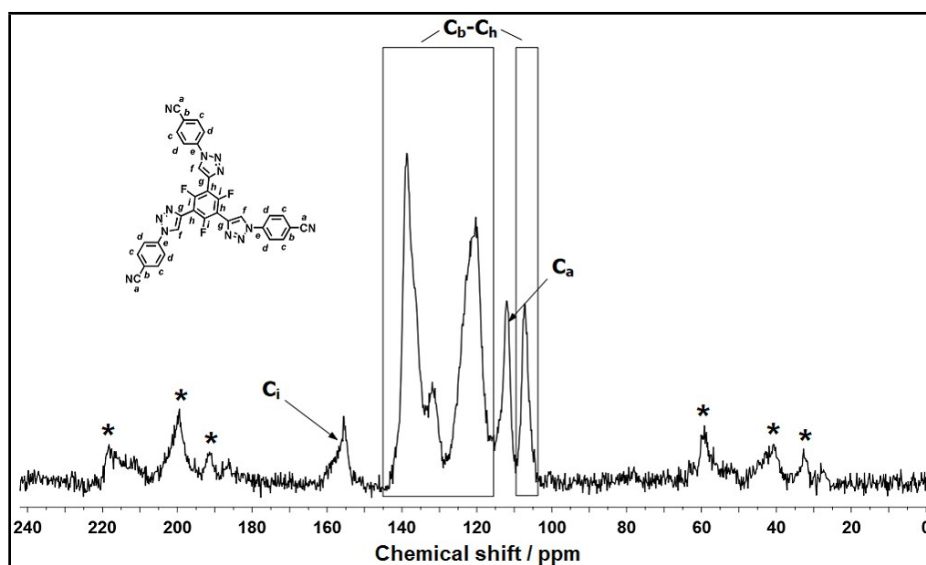
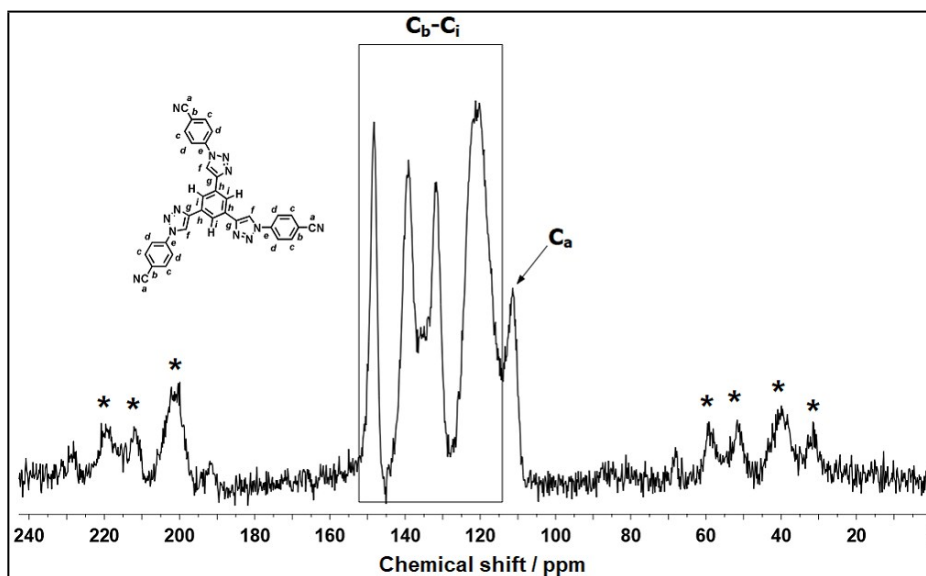


Figure S1: FT-IR spectra of Tz-FCN and TzHCN building blocks

Section D. Solid-State  $^{13}\text{C}$  CP-MAS NMR Spectroscopy:



**Figure S2:** Solid-state  $^{13}\text{C}$  CP/MAS NMR spectrum of Tz-FCN building block. Spinning side bands are starred.<sup>S6</sup>



**Figure S3:** Solid-state  $^{13}\text{C}$  CP/MAS NMR spectrum of Tz-HCN building block. Spinning side bands are starred.<sup>S6</sup>

## Section E. Powder X-ray diffraction analysis:

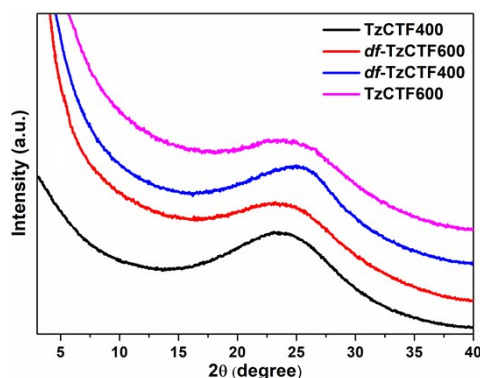


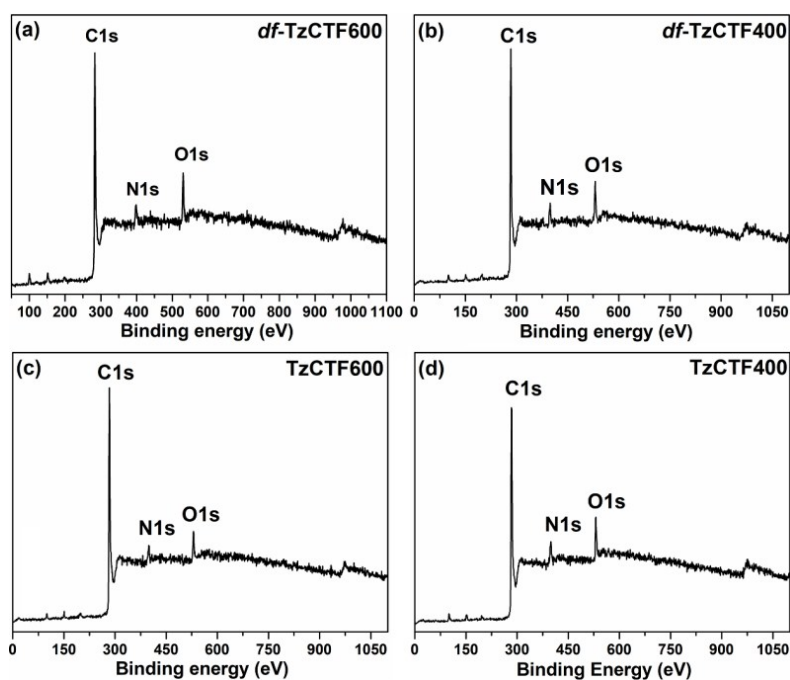
**Figure S4:** Powder X-ray diffraction spectra of all TzCTF materials.

## Section F. Elemental analysis:

**Table S1.** Elemental analysis of TzCTFs materials from combustion process

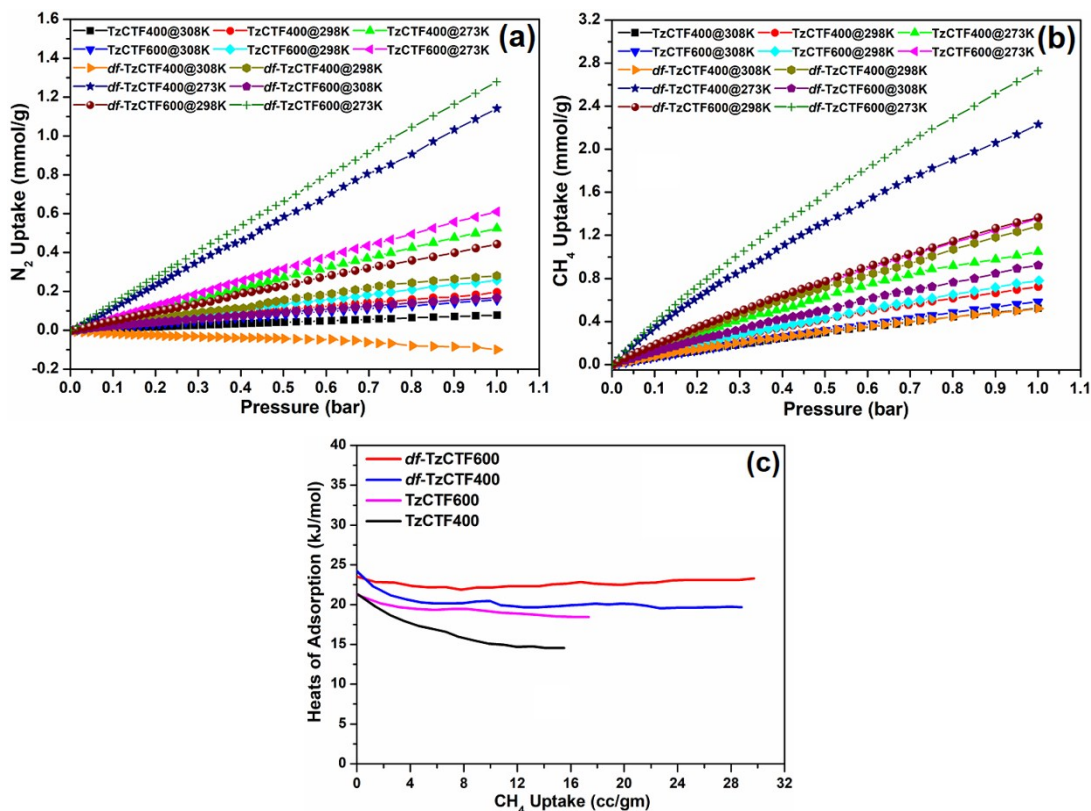
Sample	Elemental Analysis (Experimental)			C/N	C/H
	C	N	H		
TzCTF400	69.17	7.89	2.61	8.76	26.50
TzCTF600	67.56	7.05	2.16	9.58	31.15
<i>df</i> -TzCTF400	63.24	8.97	2.13	7.05	29.70
<i>df</i> -TzCTF600	60.83	8.26	2.01	7.36	28.29
Calc. Tz-HCN	68.03	28.85	3.11	2.35	21.87

## Section G. XPS survey scan:



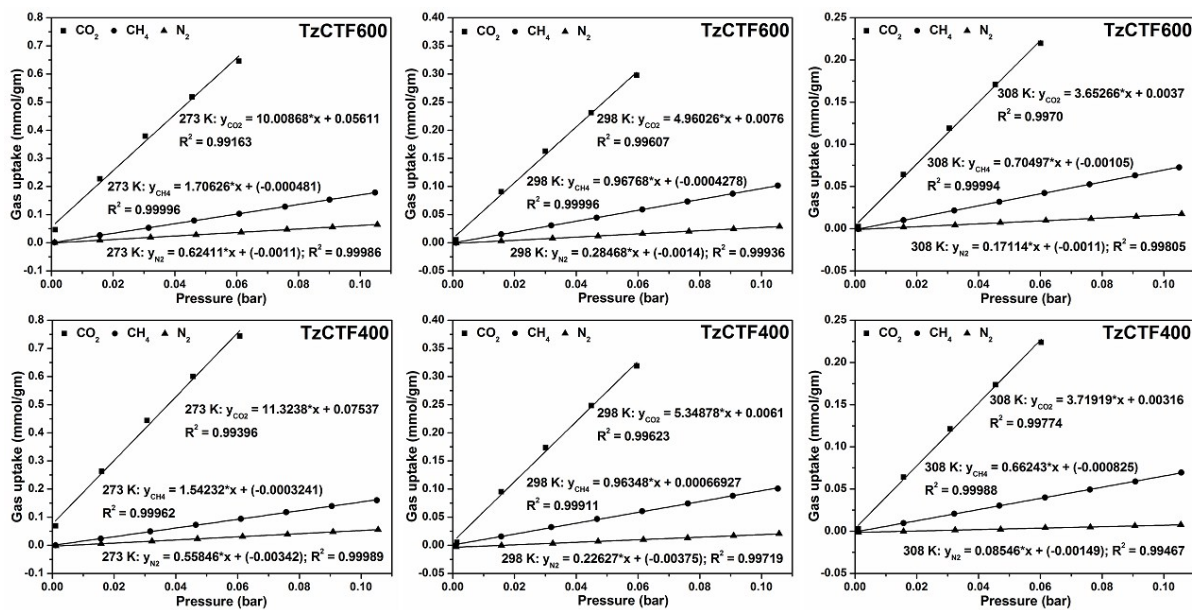
**Figure S5:** XPS survey spectra (a–d) of TzCTFs

## Section H. Pure component isotherms of N<sub>2</sub> and CH<sub>4</sub>:



**Figure S6:** (a) N<sub>2</sub> adsorption, (b) CH<sub>4</sub> adsorption of TzCTF series measure at 273 K, 298 K, and 308 K under 1 bar and (c) Isothermic heat of adsorption for TzCTFs derived from CH<sub>4</sub> adsorption isotherms at 273 K and 298 K

## Section I. Henry plots for CO<sub>2</sub>, N<sub>2</sub>, and CH<sub>4</sub>:



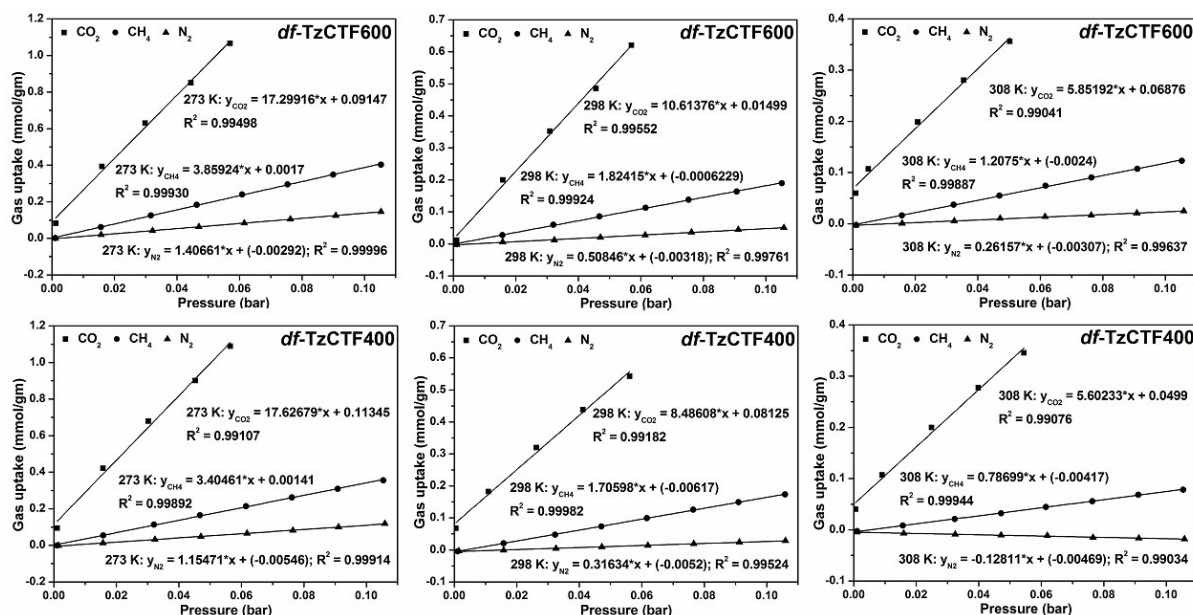


**Figure S7:** Henry plots of all TzCTF materials as derived from CO<sub>2</sub>, N<sub>2</sub>, and CH<sub>4</sub> isotherms at T = 273, 298, and 308 K.

### Section J. Henry selectivity:

**Table S2.** CO<sub>2</sub>/N<sub>2</sub> and CO<sub>2</sub>/CH<sub>4</sub> selectivity measured on the TzCTF materials at T = 273, 298, and 308 K

Temp.	Initial slope of TzCTF series materials											
	TzCTF400			TzCTF600			df-TzCTF400			df-TzCTF600		
	CO <sub>2</sub>	CH <sub>4</sub>	N <sub>2</sub>	CO <sub>2</sub>	CH <sub>4</sub>	N <sub>2</sub>	CO <sub>2</sub>	CH <sub>4</sub>	N <sub>2</sub>	CO <sub>2</sub>	CH <sub>4</sub>	N <sub>2</sub>
273K	11.323	1.542	0.558	10.008	1.706	0.624	17.626	3.404	1.154	17.299	3.859	1.406
298K	5.348	0.963	0.226	4.960	0.967	0.284	8.486	1.705	0.316	10.613	1.824	0.508
308K	3.719	0.662	0.085	3.652	0.705	0.171	5.602	0.786	(-ve)	5.852	1.207	0.261
Temp.	Henry selectivity of TzCTF series materials by initial slop method <sup>a</sup>											
	TzCTF400		TzCTF600		df-TzCTF400		df-TzCTF600					
	CO <sub>2</sub> /CH <sub>4</sub>	CO <sub>2</sub> /N <sub>2</sub>	CO <sub>2</sub> /CH <sub>4</sub>	CO <sub>2</sub> /N <sub>2</sub>	CO <sub>2</sub> /CH <sub>4</sub>	CO <sub>2</sub> /N <sub>2</sub>	CO <sub>2</sub> /CH <sub>4</sub>	CO <sub>2</sub> /N <sub>2</sub>	CO <sub>2</sub> /CH <sub>4</sub>	CO <sub>2</sub> /N <sub>2</sub>		
273K	7.342	20.276	5.865	16.036	5.177	15.265	4.482	12.298				
298K	5.551	23.638	5.125	17.424	4.974	26.78	5.818	20.868				
308K	5.614	43.519	5.181	21.343	7.118	ND	4.846	22.37				

ND: not determined as the initial slope is negative, <sup>a</sup>The selectivity of all TzCTF materials was measured from the ratio of the initial slopes in the Henry region of the respective CO<sub>2</sub>, N<sub>2</sub>, and CH<sub>4</sub> adsorption isotherms at T = 273, 298, and 308 K. The slopes of adsorption isotherms are obtained for each material by linear curve fitting as displayed in Figure S7.

### Section K. Fitting of pure component isotherms:

The experimentally measured excess loadings of CO<sub>2</sub>, and N<sub>2</sub>, obtained at three different temperatures, 273 K, 298 K, and 308 K, were first converted to absolute loadings before data fitting. The data for both adsorption and desorption cycles were included in the data fitting. The procedure for converting to absolute loadings is the same as described in the Supporting Information accompanying the paper of Wu et al.<sup>S7</sup> For the purpose of converting to absolute loadings, the pore volumes used are specified in Table S3.

The isotherm data for CO<sub>2</sub> were fitted with the dual-site Langmuir model

$$q = q_{A,sat} \frac{b_A p}{1 + b_A p} + q_{B,sat} \frac{b_B p}{1 + b_B p} \quad (1)$$

The Langmuir fit parameters for adsorption of CO<sub>2</sub> are provided in Table S4 for *df*-TzCTF600, *df*-TzCTF400, TzCTF600, and TzCTF400. The simpler Langmuir model was adequate for fitting the isotherm data for N<sub>2</sub>; Table S5 provides the Langmuir parameters for N<sub>2</sub> for *df*-TzCTF600, *df*-TzCTF400, TzCTF600, and TzCTF400. The isotherm fits are excellent for all four materials at all temperatures. This is demonstrated in the comparisons of experimental data and the isotherm fits for *df*-TzCTF600, *df*-TzCTF400, TzCTF600, and TzCTF400 in Figure S8.

#### Section L. Isostatic heat of adsorption:

The isosteric heat of adsorption,  $Q_{st}$ , defined as

$$Q_{st} = RT^2 \left( \frac{\partial \ln p}{\partial T} \right)_q \quad (2)$$

were determined using the pure component isotherm fits using the Clausius-Clapeyron equation. Figure S9 presents a comparison of the isosteric heats of adsorption of CO<sub>2</sub> in *df*-TzCTF600, *df*-TzCTF400, TzCTF600, and TzCTF400 as a function of the CO<sub>2</sub> loading. The heats of adsorption of all four materials are close to one another.

#### Section M. IAST calculations of adsorption selectivities and uptake capacities:

The selectivity of preferential adsorption of component 1 over component 2 in a mixture containing 1 and 2, perhaps in the presence of other components too, can be formally defined as

$$S_{ads} = \frac{q_1/q_2}{p_1/p_2} \quad (3)$$

In equation (3),  $q_1$  and  $q_2$  are the *absolute* component loadings of the adsorbed phase in the mixture. These component loadings are also termed the uptake capacities. In all the calculations to be presented below, the calculations of  $q_1$  and  $q_2$  are based on the use of the Ideal Adsorbed Solution Theory (IAST) of Myers and Prausnitz.<sup>S8</sup>

For 15/85 mixtures, the IAST calculations of CO<sub>2</sub> and N<sub>2</sub> uptakes at 298 K in *df*-TzCTF600, *df*-TzCTF400, TzCTF600, and TzCTF400 are compared in Figure S10. We note that the uptake of both guest molecules is highest in *df*-TzCTF600 mainly because of its higher pore volume. The lowest CO<sub>2</sub> uptakes are for TzCTF400 and TzCTF600.

Figure S11 presents the values of the CO<sub>2</sub>/N<sub>2</sub> adsorption selectivity for 15/85 flue gas mixture at 298 K using equation (3). We note that the CO<sub>2</sub>/N<sub>2</sub> adsorption selectivity is highest for *df*-TzCTF400 and lowest for TzCTF600.

#### **Section N. Transient breakthrough simulations in fixed bed adsorbers:**

The separation of CO<sub>2</sub>/N<sub>2</sub> mixtures is commonly carried out in fixed bed adsorbers in which the separation performance is dictated by a combination of three separate factors: (a) adsorption selectivity, and (b) uptake capacity. For a proper comparison of the performance of *df*-TzCTF600, *df*-TzCTF400, TzCTF600, and TzCTF400, we carried out transient breakthrough simulations that are representative of industrial fixed bed operations. The simulation methodology is as described in earlier publications.<sup>94-96</sup> For all the breakthrough calculations reported in this work, we assume negligible diffusion resistances for all materials

In order to evaluate the different adsorbents for use in a PSA unit, breakthrough calculations were performed using fixed beds of identical dimensions. The bulk densities of the packed materials are as specified in Table S3. For the breakthrough simulations, the following parameter values were used: length of packed bed,  $L = 0.3$  m; voidage of packed bed,  $L = 0.4$ ; superficial gas velocity at inlet,  $u = 0.04$  m/s. The characteristic contact time between the adsorbent and the surrounding gas phase is  $L\varepsilon/u$ . It is common to use the dimensionless time,  $\tau = tu/L\varepsilon$ , obtained by dividing the actual time,  $t$ , by the characteristic time,  $L\varepsilon/u$  when plotting simulated breakthrough curves. The operating temperature is 298 K and the total pressure is 1 bar. The partial pressures of CO<sub>2</sub> and N<sub>2</sub> at the feed gas inlet are 15 kPa, and 85 kPa, respectively.

The breakthrough calculations for *df*-TzCTF600, *df*-TzCTF400, TzCTF600, and TzCTF400 are compared in Figure 10 (main text). The  $y$ -axis in the plot is the concentration of the component in the outlet gas stream, normalized with respect the inlet composition.

A longer breakthrough time for CO<sub>2</sub> indicates better separation performance because more of CO<sub>2</sub> can be adsorbed in the bed before the need for regeneration. The best separations are achieved with *df*-TzCTF600. The reason for its good separation is mainly attributable to its high CO<sub>2</sub> uptake capacity (as noted in Figure S3), in combination with reasonably high CO<sub>2</sub>/N<sub>2</sub> adsorption selectivity (see Figure S4). The poorest separation is achieved with TzCTF600, and the reason for its poor performance is due to the low CO<sub>2</sub> uptake capacity (see Figure S3), in combination with low CO<sub>2</sub>/N<sub>2</sub> adsorption selectivity (see Figure S4).

**Section O. Notation used in breakthrough simulation:**

$b$	Langmuir constant for species $i$ at adsorption, Pa <sup>-1</sup>
$c_i$	molar concentration of species $i$ in gas mixture, mol m <sup>-3</sup>
$c_{i0}$	molar concentration of species $i$ in gas mixture at inlet to adsorber, mol m <sup>-3</sup>
$L$	length of packed bed adsorber, m
$p_i$	partial pressure of species $i$ in mixture, Pa
$p_t$	total system pressure, Pa
$q_i$	component molar loading of species $i$ , mol kg <sup>-1</sup>
$t$	time, s
$T$	absolute temperature, K
$u$	superficial gas velocity in packed bed, m s <sup>-1</sup>

**Greek letters**

$\varepsilon$	voidage of packed bed, dimensionless
$\rho$	framework density, kg m <sup>-3</sup>
$\tau$	time, dimensionless

**Subscripts**

$i$	referring to component $i$
$t$	referring to total mixture

**Section P. Supporting tables:**

**Table S3.** Salient properties of  $df$ -TzCTF600,  $df$ -TzCTF400, TzCTF600, and TzCTF400.

Material	Bulk density (g cm <sup>-3</sup> )	Pore volume (cm <sup>3</sup> g <sup>-1</sup> )
$df$ -TzCTF600	0.337	1.124
$df$ -TzCTF400	0.292	0.7057
TzCTF600	0.348	1.02
TzCTF400	0.544	0.6949

**Table S4.** Dual-site Langmuir parameters for adsorption of CO<sub>2</sub> in  $df$ -TzCTF600,  $df$ -TzCTF400, TzCTF600, and TzCTF400. The experimentally measured excess loadings were first converted to absolute loadings before data fitting.

Material	Temperature $T$ / K	Site A		Site B	
		$q_{A,sat}$ mol kg <sup>-1</sup>	$b_A$ Pa <sup>-1</sup>	$q_{B,sat}$ mol kg <sup>-1</sup>	$B_B$ Pa <sup>-1</sup>
$df$ -TzCTF600	273 K	0.9	$2.63 \times 10^{-4}$	15.5	$6.22 \times 10^{-6}$
$df$ -TzCTF600	298 K	0.9	$1.12 \times 10^{-4}$	15.5	$3.16 \times 10^{-6}$

<i>df</i> -TzCTF600	308 K	0.9	$5.43 \times 10^{-5}$	15.5	$1.74 \times 10^{-6}$
<i>df</i> -TzCTF400	273 K	1.4	$1.91 \times 10^{-4}$	9.8	$7.33 \times 10^{-6}$
<i>df</i> -TzCTF400	298 K	1.4	$6.94 \times 10^{-5}$	9.8	$2.75 \times 10^{-6}$
<i>df</i> -TzCTF400	308 K	1.4	$3.9 \times 10^{-5}$	9.8	$1.43 \times 10^{-6}$
TzCTF600	273 K	0.7	$1.71 \times 10^{-4}$	11.4	$4.91 \times 10^{-6}$
TzCTF600	298 K	0.7	$5.24 \times 10^{-5}$	11.4	$2.1 \times 10^{-6}$
TzCTF600	308 K	0.7	$3.44 \times 10^{-5}$	11.4	$1.55 \times 10^{-6}$
TzCTF400	273 K	1.05	$1.3 \times 10^{-4}$	8.1	$6.74 \times 10^{-6}$
TzCTF400	298 K	1.05	$3.44 \times 10^{-5}$	8.1	$2.71 \times 10^{-6}$
TzCTF400	308 K	1.05	$2.15 \times 10^{-5}$	8.1	$1.96 \times 10^{-6}$

**Table S5.** Single-site Langmuir parameters for N<sub>2</sub> in *df*-TzCTF600, *df*-TzCTF400, TzCTF600, and TzCTF400.

Material	Temperature <i>T</i> / K	$q_{A,sat}$ (mol kg <sup>-1</sup> )	$b_A$ (Pa <sup>-1</sup> )
<i>df</i> -TzCTF600	273 K	15	$9.48 \times 10^{-7}$
<i>df</i> -TzCTF600	298 K	15	$3.32 \times 10^{-7}$
<i>df</i> -TzCTF600	308 K	15	$1.49 \times 10^{-7}$
<i>df</i> -TzCTF400	273 K	7	$1.9 \times 10^{-6}$
<i>df</i> -TzCTF400	298 K	7	$4.42 \times 10^{-7}$
TzCTF600	273 K	13	$5.34 \times 10^{-7}$
TzCTF600	298 K	13	$2.25 \times 10^{-7}$
TzCTF600	308 K	13	$1.65 \times 10^{-7}$
TzCTF400	273 K	15	$3.8 \times 10^{-7}$
TzCTF400	298 K	15	$1.5 \times 10^{-7}$
TzCTF400	308 K	15	$7.0 \times 10^{-8}$

**Table S6.** Comparison of surface area, CH<sub>4</sub> uptake (> 2 wt% at 273 K) and  $Q_{st}$  of other high-performing POP and CTF based adsorbents at 1 bar.

POP & CTF-based adsorbents	$S_{BET}$ (m <sup>2</sup> g <sup>-1</sup> )	CH <sub>4</sub> Uptake [wt%]		$Q_{st}$ [KJ mol <sup>-1</sup> ]	Ref.
	77K	273 K	298 K		
TPC-1	1940	6.2	-	-	<b>60</b>
<i>df</i> -TzCTF600	1720	4.38	2.18	23.5	Current work
<i>df</i> -TzCTF400	906	3.57	2.06	24.2	Current work
TzCTF600	1582	2.17	1.24	21.2	Current work
TzCTF400	874	1.68	1.15	21.3	Current work
PPOP-1	720	4.01	-	-	<b>S15</b>
PPOP-2	920	4.29	-	-	
PPOP-3	880	3.24	-	-	
BDT-3	1010	2.9	-	-	<b>S16</b>

BILP-6-NH <sub>2</sub>	1185	2.8	-	-	<b>S17</b>
TPMTP	890	2.7	-	-	<b>S18</b>
PCTF-4	1404	2.7	-	-	<b>24</b>
BILP-6	1261	2.7	1.90	13.2	<b>S19</b>
BILP-3	1306	2.4	1.70	16.6	
ALP-1	1235	2.6	1.50	20.8	<b>S20</b>
Cz-POF-3	1927	2.54	1.71 <sup>a</sup>	20.2	<b>S21</b>
Cz-POF-1	2065	2.29	1.56 <sup>a</sup>	19	
BILP-4	1135	2.53	1.80	13.0	<b>S22</b>
PPF-1	1740	2.43	-	15.1	<b>96</b>
PPF-2	1470	2.31	-	15.9	
BILP-12	1497	2.4	1.50	18.6	<b>S23</b>
TNP-4	1348	2.38	1.42	20	<b>S24</b>
MM2	1360	2.34	1.51 <sup>b</sup>	-	<b>51</b>
MM1	1800	2.06	1.34 <sup>b</sup>	-	
CTF-TPC	1668	2.14	-	-	<b>S14</b>
PAF-60	1094	2.0	1.50	24.1	<b>S25</b>
JUC-Z8	4743	2.0	-	-	<b>S26</b>

<sup>a</sup>measured at 290 K. <sup>b</sup>measured at 293 K

**Table S7.** Comparison of structural parameters, CO<sub>2</sub> (> 4 mmol g<sup>-1</sup> at 273 K) and H<sub>2</sub> uptakes, and CO<sub>2</sub>/N<sub>2</sub> selectivity of TzCTFs materials with other most representative related CTF-based adsorbents

CTF-based adsorbents	S <sub>BET</sub> (m <sup>2</sup> g <sup>-1</sup> )	CO <sub>2</sub> Uptake [mmol g <sup>-1</sup> ]				Q <sub>st</sub> [KJ mol <sup>-1</sup> ]	Selectivity <sup>298 K</sup> (CO <sub>2</sub> /N <sub>2</sub> )		H <sub>2</sub> Uptake [wt%]	Ref.
	77 K	273 K	298 K	308 K	Henry		IAST	77 K		
<i>df</i> -TzCTF600	1720	6.79	4.60	3.00	34	17	30	2.50	Current work	
<i>df</i> -TzCTF400	906	5.51	3.32	2.32	35	22	40	2.16	Current work	
TzCTF600	1582	4.40	2.51	2.03	28	16	21	2.06	Current work	
TzCTF400	874	4.21	2.55	1.90	32	21	26	1.75	Current work	
HAT-CTF 450/600	1090	6.3	-	-	27.1	-	-	-	<b>23</b>	
HAT-CTF-600	899	5.1	-	-	-	-	-	-		
HAT-CTF-450	756	4.4	-	-	-	-	-	-		
F-DCBP-CTF-1	2437	5.98	3.82	-	33.1	31	-	1.77	<b>57</b>	
F-DCBP-CTF-2	2036	5.23	3.16	-	-	22	-	-		
CTF-py	1239	5.08	3.79	-	35.1	45	-	1.63	<b>95</b>	
CTF-ph	1991	4.54	3.05	-	33.2	20	-	1.87		
<i>bipy</i> -CTF500	1548	5.34	3.07	1.77 <sup>a</sup>	34.2	61	42	1.63	<b>56</b>	
<i>bipy</i> -CTF600	2479	5.58	2.95	1.84 <sup>a</sup>	34.4	37	24	2.10		
<i>lut</i> -CTF350	635	4.06	2.41	1.59 <sup>a</sup>	37.4	76	66	1.22		

<i>lut</i> -CTF400	968	4.55	2.72	1.80 <sup>a</sup>	37.5	63	53	1.36	
<i>lut</i> -CTF500	1680	5.04	2.58	1.71 <sup>a</sup>	38.2	27	27	1.60	
<i>lut</i> -CTF600	2815	4.99	2.52	1.66 <sup>a</sup>	33.3	26	23	2.00	
FCTF-1-600	1535	5.53	3.41	-	-	-	19	-	<b>55</b>
FCTF-1	662	4.67	3.21	-	35	-	31	-	
<i>p</i> CTF-1	2034	4.97	-	-	25.9	-	-	1.75	<b>S9</b>
TPC-1	1940	4.90	-	-	39	38 <sup>b</sup>	-	2.00	<b>60</b>
MM2	1360	4.77	-	-	32	23 <sup>b</sup>	44 <sup>b</sup>	1.74	<b>51</b>
PCTF-4	1404	4.65	2.86	-	~31	56 <sup>b</sup>	-	1.30	<b>24</b>
<i>fl</i> -CTF-350	1235	4.28	2.29	1.59 <sup>a</sup>	32.7	27	23	-	<b>21</b>
<i>fl</i> -CTF-400	2862	4.13	1.97	1.31 <sup>a</sup>	30.7	15	16	1.95	
CTF-0	2011	4.22	-	-	-	-	-	-	<b>22</b>
P6M	947	4.17	-	-	-	-	14.2 <sup>b</sup>	-	<b>S10</b>
PCTP-1	1200	4.91	3.24	2.56 <sup>c</sup>	44.5	46.1	-	-	<b>S11</b>
CTF-BI-4	1025	4.85	-	2.72 <sup>c</sup>	34.3–3 1.7	44.0 <sup>b</sup>	-	-	<b>S12</b>
CTF-BI-5	836	4.49	-	2.68 <sup>c</sup>		35.6 <sup>b</sup>	-	-	
CTF-BI-9	885	4.29	-	2.36 <sup>c</sup>		67.4 <sup>b</sup>	-	-	
CTF-BI-10	1099	4.45	-	2.58 <sup>c</sup>		31.3 <sup>b</sup>	-	-	
CTF-BI-11	1549	4.93	-	2.63 <sup>c</sup>		34.3 <sup>b</sup>	-	-	
MCTP-1	1452	4.64	2.69	1.82	40.0	15.4	-	-	<b>S13</b>
CTF-TPC	1668	4.25			32	20.0 <sup>b</sup>	30.0 <sup>b</sup>	1.75	<b>S14</b>

<sup>a</sup>measured at 313 K, <sup>b</sup>measured at 273 K. <sup>c</sup>measured at 303 K

### Section Q. Supporting figures:

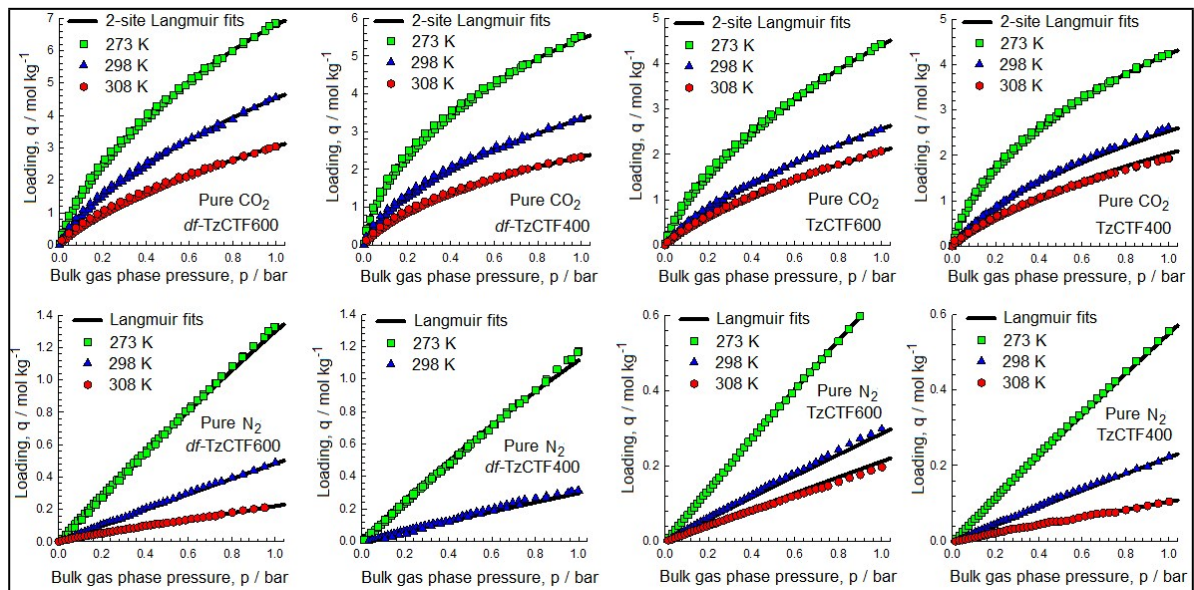


**Figure S8.** Comparison of the pure component isotherm data in *df*-TzCTF600, *df*-TzCTF400, TzCTF600, and TzCTF400 with the fitted isotherms (shown by continuous solid lines) at various temperatures.

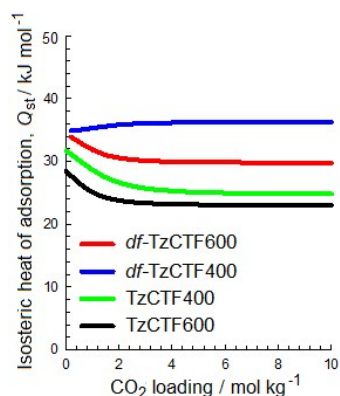


**Figure S9.** Comparisons of the isosteric heats of adsorption of CO<sub>2</sub> in *df*-TzCTF600, *df*-TzCTF400, TzCTF600, and TzCTF400 as a function of the CO<sub>2</sub> loading.

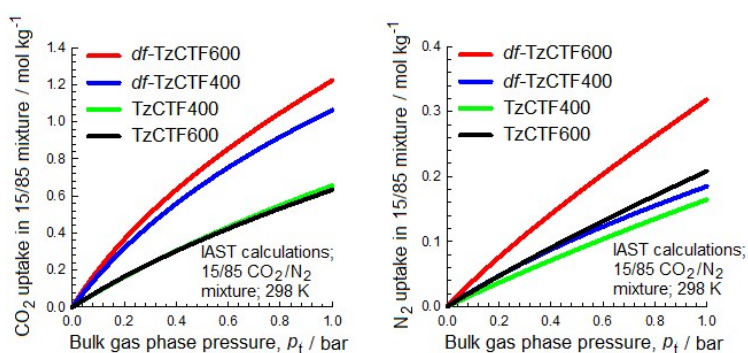


**Figure S10.** Calculations using Ideal Adsorbed Solution Theory (IAST) of Myers and Prausnitz<sup>S8</sup> for uptakes of CO<sub>2</sub> and N<sub>2</sub> expressed as moles per kg of adsorbent, in equilibrium with binary CO<sub>2</sub>/N<sub>2</sub> gas mixture maintained at isothermal conditions at 298 K. In these calculations the partial pressures of CO<sub>2</sub> and N<sub>2</sub> are taken to be  $p_1/p_2 = 15/85$ .

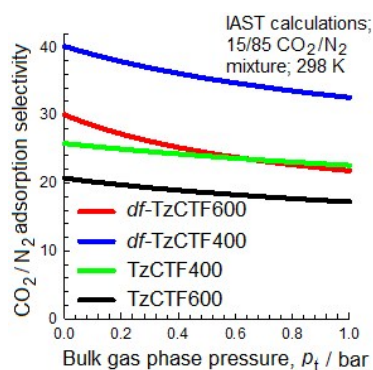


**Figure S11.** Calculations using Ideal Adsorbed Solution Theory (IAST) of Myers and Prausnitz<sup>S8</sup> for CO<sub>2</sub>/N<sub>2</sub> adsorption selectivity for a binary CO<sub>2</sub>/N<sub>2</sub> gas mixture maintained at isothermal conditions at 298 K. In these calculations the partial pressures of CO<sub>2</sub> and N<sub>2</sub> are taken to be  $p_1/p_2 = 15/85$ .

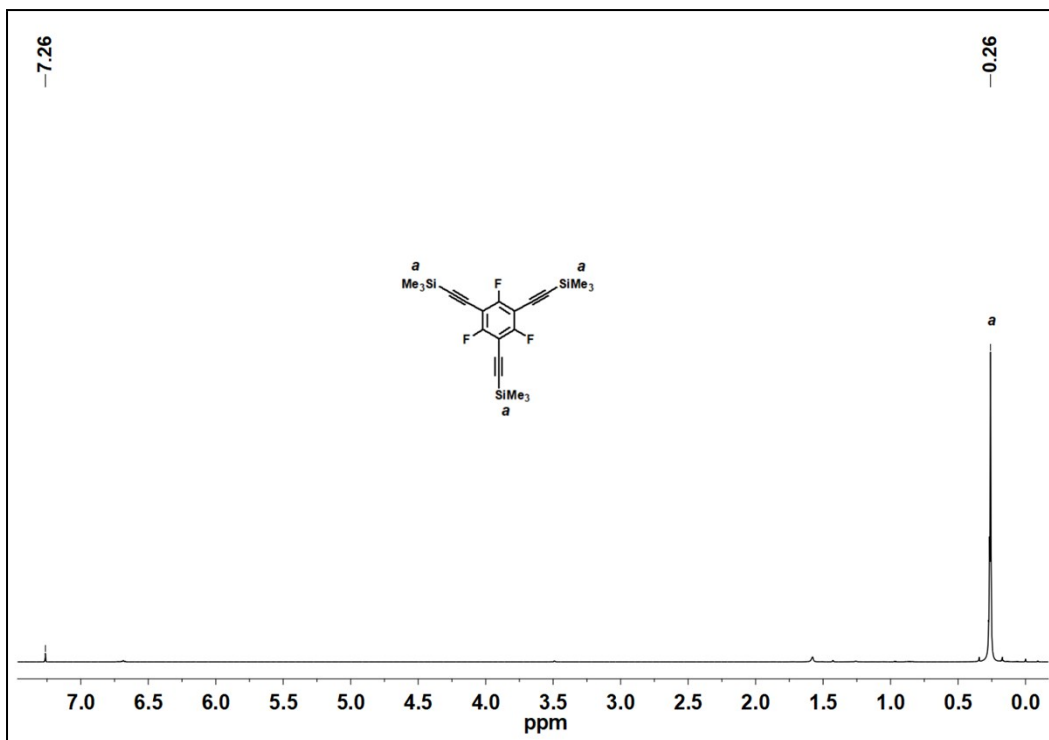


**Figure S12:**  $^1\text{H}$  NMR of 1,3,5-trifluoro-2,4,6-tris[(trimethylsilyl)ethynyl]benzene

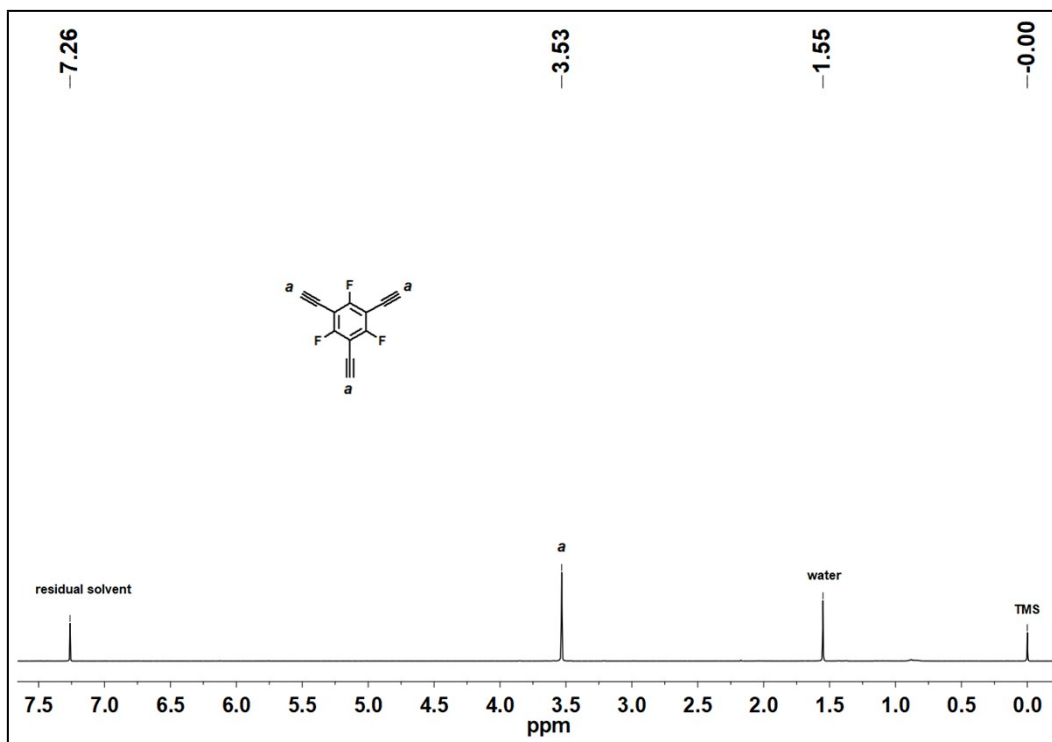


**Figure S13:**  $^1\text{H}$  NMR of 1,3,5-triethynyl-2,4,6-trifluorobenzene

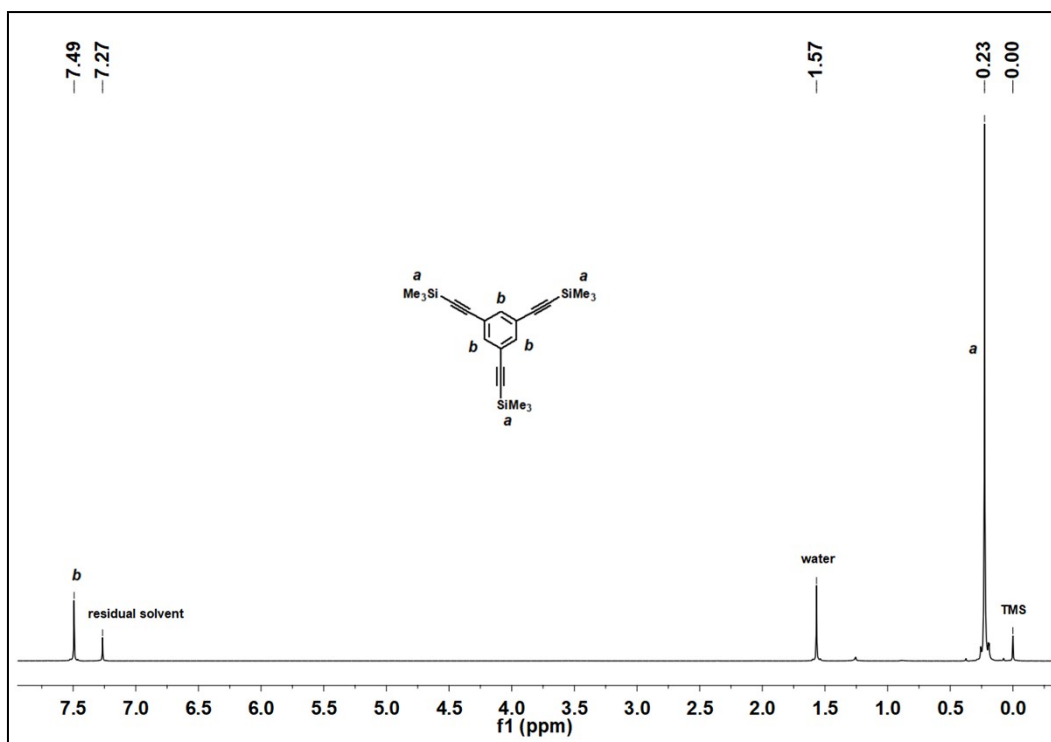


Figure S14:  $^1\text{H}$  NMR of 1,3,5-tris[2-(trimethylsilyl)ethynyl]benzene

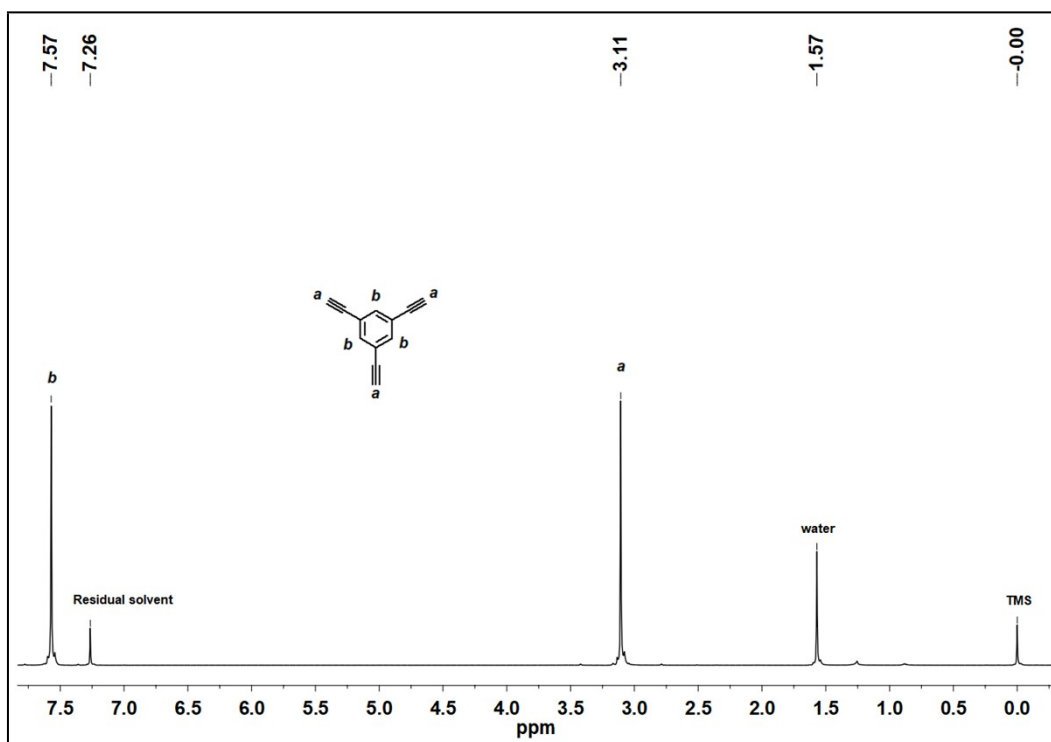
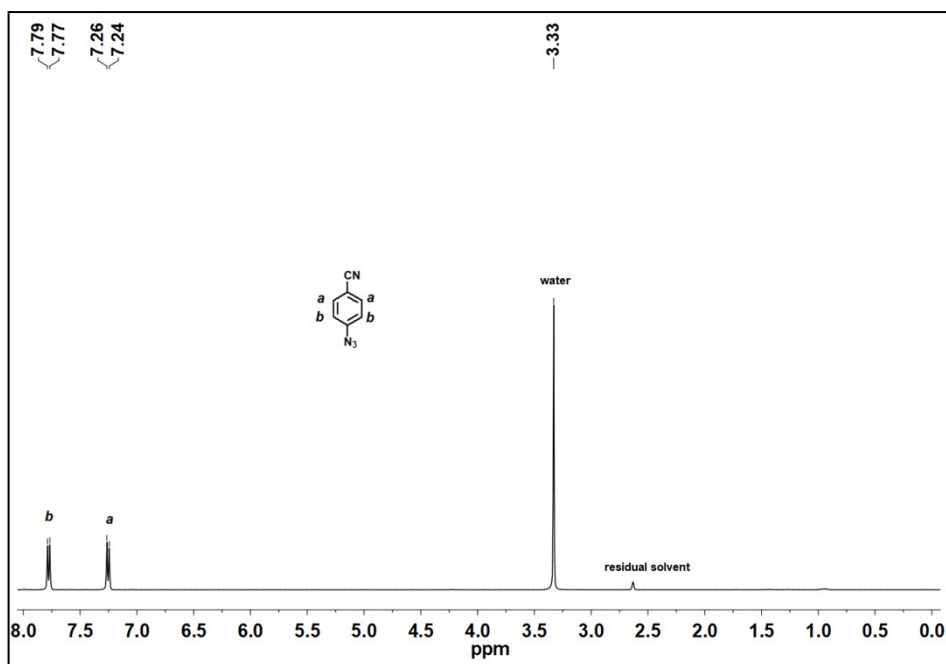


Figure S15:  $^1\text{H}$  NMR of 1,3,5-triethynylbenzene



**Figure S16:**  $^1\text{H}$  NMR of 4-azidobenzonitrile.

As per the reviewer comment, soluble model compound (**MC-1**) has been synthesized to justify further the successful formation of current building blocks Tz-HCN and Tz-FCN via “click reaction”.

### Section R. Structure, synthesis, and characterization of Model Compounds:

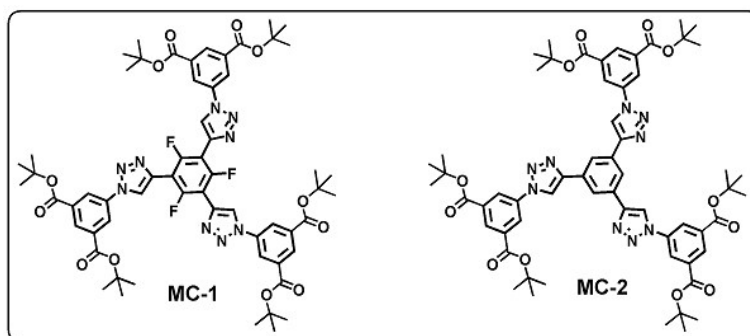
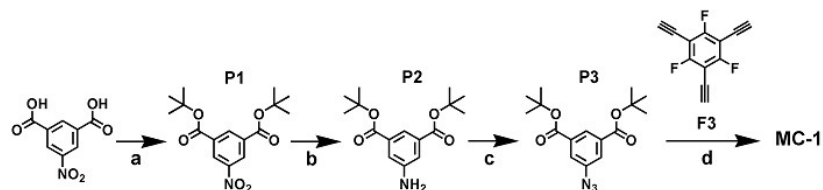


**Chart S1:** Chemical structure of model compound, **MC-1** and **MC-2**. The synthesis of **MC-2** is already reported by X.-J. Wang et al. in *Scientific Report*, 2013, **3**, 1149.<sup>S27</sup>



**Scheme S2:** Synthetic route of **MC-1** (a): DMAP, DCC, tert-Butanol; (b): Pd/C, ammonium formate, MeOH; (c): HCl, sodium nitrite,  $\text{NaN}_3$ , Methanol,  $0^\circ\text{C}$ ; (d): Sodium ascorbate,  $\text{CuSO}_4 \cdot 5\text{H}_2\text{O}$ , Water, Tetrahydrofuran,  $40^\circ\text{C}$ , 3 days.

**Synthesis of Di-*tert*-butyl 5-nitroisophthalate (P1):**<sup>S28</sup> It was synthesized from 5-nitroisophthalic acid using literature method and purified by column chromatography (100% CHCl<sub>3</sub>) to get 6.3 g of white solid (65%). <sup>1</sup>H NMR (400 MHz; CDCl<sub>3</sub>): 1.64 (s, 18H), 8.92 (d, 2H), 8.87 (t, 1H)

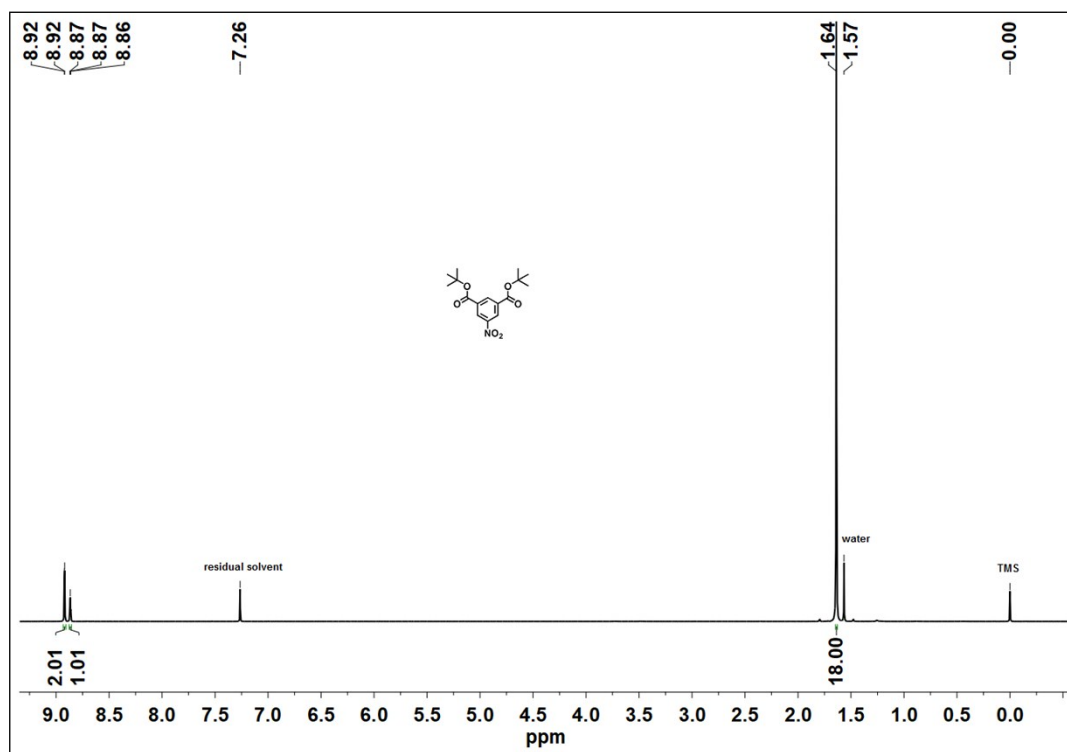


**Figure S17:** <sup>1</sup>H NMR of di-*tert*-butyl 5-nitroisophthalate, P1

**Synthesis of Di-*tert*-butyl 5-aminoisophthalate (P2):**<sup>S29</sup> It was synthesized from di-*tert*-butyl 5-nitroisophthalate using literature method with quantitative yield and the as-synthesized compound is used in next step without any further characterization.

**Synthesis of Di-*tert*-butyl 5-azidoisophthalate (P3):**<sup>S27</sup> A 250 ml round bottom flask equipped with stir bar was charged with di-*tert*-butyl 5-aminoisophthalate (4.7 g, 16.02 mmol), MeOH (175 ml) and HCl (0.5 M, 175 ml). The reaction mixture was cooled down to 0-5°C and stirred for 1 hour. Ice-cold solution of sodium nitrite (3.31 g, 48.06 mmol) was added dropwise into the reaction mixture and stirring was continued for 1 hour. Then the reaction mixture was slowly poured into a solution of NaN<sub>3</sub> (3.16 g, 48.5 mmol) at 0°C. The combined reaction mixture was then stirred for additional 1.0 hour. The reaction mixture was then extracted by dichloromethane (3 x 50 ml). The combined organic layer was washed with water and dried over anhydrous MgSO<sub>4</sub>. The organic layer was evaporated to dryness under reduced pressure to obtain crude product which was purified by silica gel column

chromatography (hexane:dichloromethane 5:5) yielding **P1** (3.84 g, 75 %) as white solid.  $^1\text{H}$  NMR (400 MHz;  $\text{CDCl}_3$ ): 1.61 (s, 18H), 7.78 (d, 2H), 8.32 (t, 3H)

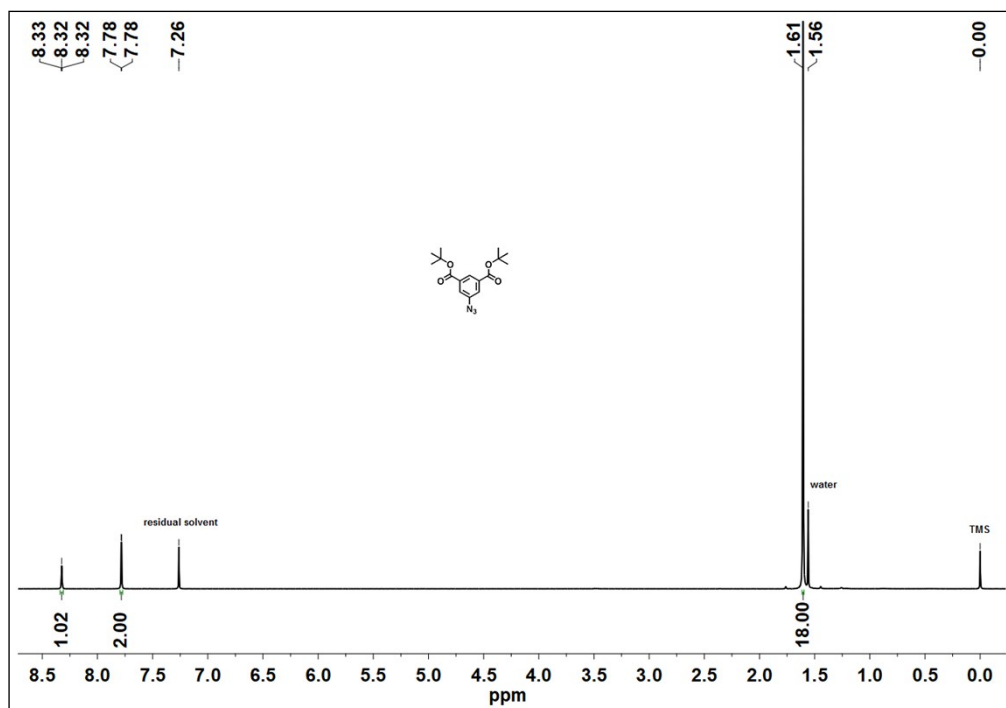


**Figure S18:**  $^1\text{H}$  NMR spectra of precursor, **P3**

**Synthesis of model compound (MC-1):** A 250 ml round bottom flask equipped with stir bar was charged with 1,3,5-triethynyl-2,4,6-trifluorobenzene, **F3** (210 mg, 1.02 mmol), di-*tert*-butyl-5-azidoisophthalate, **P3** (1.11 g, 3.49 mmol), THF (100 ml), and water (40 ml). The resulting solution was purged with argon over 30 min at room temperature followed by addition of  $\text{CuSO}_4 \cdot 5\text{H}_2\text{O}$  (80 mg, 0.32 mmol) and sodium ascorbate (127 mg, 0.64 mmol). The reaction mixture was heated to  $40^\circ\text{C}$  and kept stirring for 3 days under inert atmosphere. After completion of the reaction THF was evaporated and organic part was extracted by DCM (3 x 25 ml) and washed with water followed by drying over anhydrous  $\text{MgSO}_4$ . Organic layer was evaporated to dryness and the crude product was purified via column chromatography (silica gel, ethyl acetate:dichloromethane 0.2:9.8) to obtain cream colored solid compound (609 mg, 51%).  $^1\text{H}$  NMR (400 MHz;  $\text{CDCl}_3$ ): 1.66 (s, 54H), 8.58 (s, 3H), 8.59-8.60 (d, 6H), 8.70 (t, 3H)

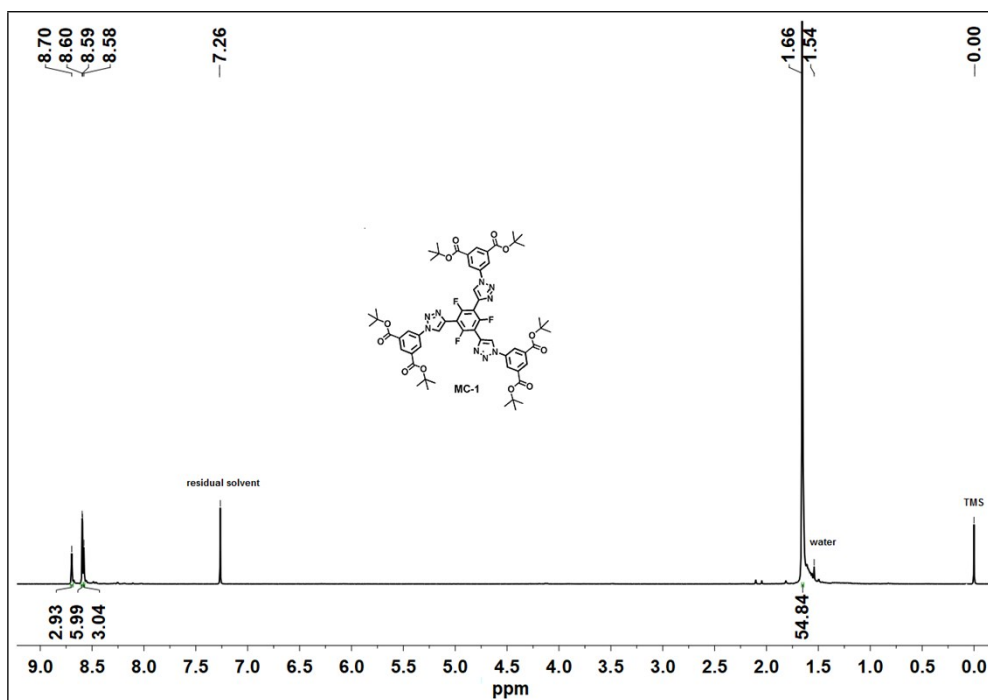


**Figure S19:**  $^1\text{H}$  NMR spectra of MC-1

As per the reviewer suggestion, TzCTFs synthesis were made at  $700^\circ\text{C}$  using both fluorinated (Tz-FCN) and non-fluorinated (Tz-HCN) building block and evaluated their textural and gas adsorption properties to further address the synthesis temperature effect on gas uptake properties in TzCTFs series materials.

### Section S. Gas uptake experiments and textural properties:

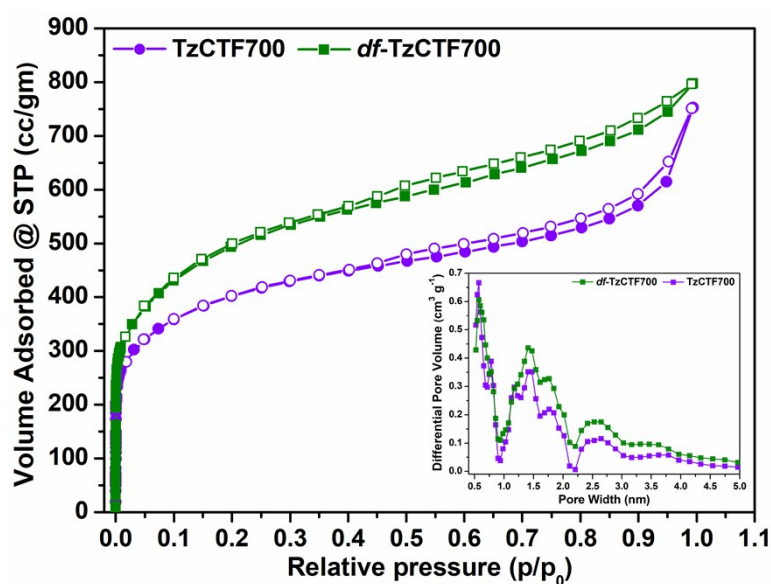


**Figure S20:** Nitrogen adsorption-desorption isotherms measured at 77 K (the solid and open symbols represent adsorption and desorption, respectively); the inset display the pore size distribution calculated by the NL-DFT method.

**Table S8:** Porosity data derived from N<sub>2</sub> isotherm (77 K, 1 bar) of TzCTFs materials synthesized at 700°C

Material	$S_{\text{BET}}^{\text{a}}$ (m <sup>2</sup> g <sup>-1</sup> )	$S_{\text{Lang}}^{\text{b}}$ (m <sup>2</sup> g <sup>-1</sup> )	$V_{0.1}^{\text{c}}$ (cm <sup>3</sup> g <sup>-1</sup> )	$V_{\text{tot}}^{\text{d}}$ (cm <sup>3</sup> g <sup>-1</sup> )	$V_{0.1}/V_{\text{tot}}$	$V_{\text{micro}}^{\text{e}}$ (CO <sub>2</sub> ) (cm <sup>3</sup> g <sup>-1</sup> )
<b><i>df</i>-TzCTF700</b>	1628	1921	0.66	1.24	0.53	0.040
<b>TzCTF700</b>	1307	1582	0.55	1.16	0.47	0.033

<sup>a</sup>Calculated BET surface area over the pressure range 0.05-0.3  $P/P_0$ . <sup>b</sup>Langmuir surface area calculated by applying Langmuir equation on nitrogen adsorption isotherm over the pressure range 0-0.15  $P/P_0$ . (c) Micropore volume calculated at  $P/P_0 = 0.1$  for pores with diameter smaller than 1.6 nm. (d) Total pore volume calculated at  $P/P_0 = 0.99$ . (e) Total pore volume for pores with diameters smaller than 0.9 nm at  $P/P_0 = 0.1$  calculated from CO<sub>2</sub> adsorption isotherm at 273 K (NL-DFT model).

**Table S9:** Gas uptake properties for the presented TzCTF materials synthesized at 700°C

Material	CO <sub>2</sub> Uptake <sup>a</sup>			CH <sub>4</sub> Uptake <sup>c</sup>		H <sub>2</sub> Uptake <sup>c</sup>
	273 K	298 K	$Q_{\text{st}}^{\text{b}}$	273 K	298 K	77 K
<b><i>df</i>-TzCTF700</b>	4.68 (1.16)	3.04	25	1.96	1.26	2.12
<b>TzCTF700</b>	4.06 (0.95)	2.55	31	1.46	0.98	1.67

<sup>a</sup>Gas uptake in mmol g<sup>-1</sup> at 1 bar and values in parenthesis in mmol g<sup>-1</sup> at 0.15 bar, <sup>b</sup>Isosteric heat of adsorption at zero coverage in kJ mol<sup>-1</sup>, <sup>c</sup>Gas uptake in wt% at 1 bar.

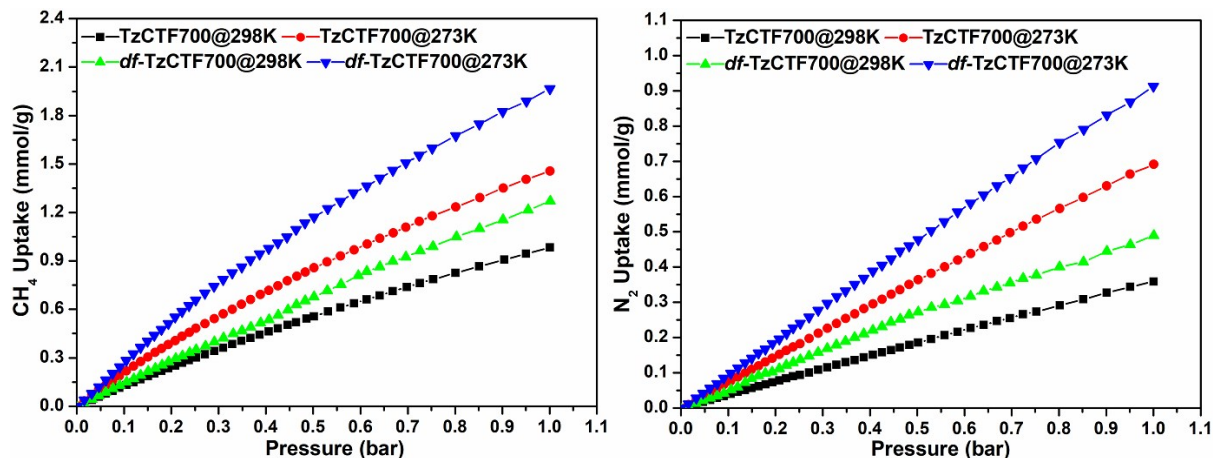


**Figure S21:** (a) CH<sub>4</sub> adsorption (left) and (b) N<sub>2</sub> adsorption (right) of *df*-TzCTF700 and TzCTF700 material measured at 273 K and 298 K under 1 bar

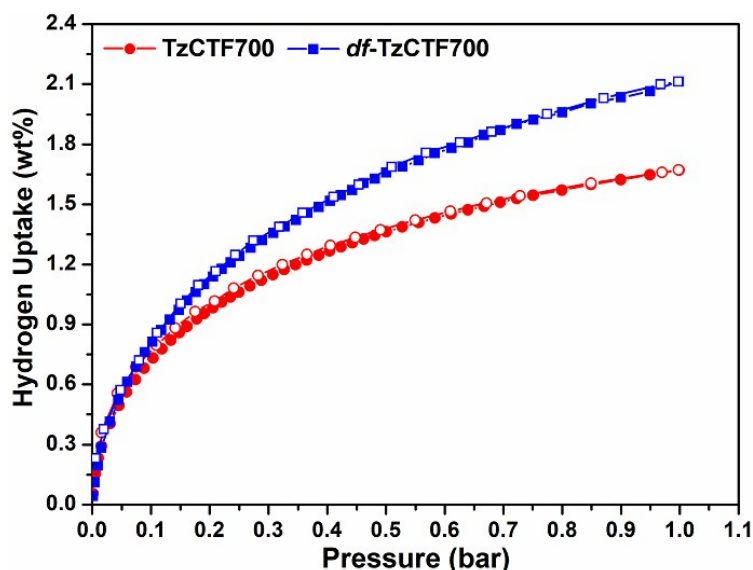


**Figure S22:** (a) H<sub>2</sub> adsorption-desorption isotherm of *df*-TzCTF700 and TzCTF700 material measured at 77 K under 1 bar

**Table S10:** Comparison of textural and gas adsorption properties of our highest performing *df*-TzCTF600 material with other high-performing related CTF-based materials

CTF-based adsorbents	S <sub>BET</sub> (m <sup>2</sup> g <sup>-1</sup> )	S <sub>micro</sub> (m <sup>2</sup> g <sup>-1</sup> )	V <sub>micro</sub> [cm <sup>3</sup> g <sup>-1</sup> ]	CO <sub>2</sub> Uptake [mmol g <sup>-1</sup> ]		CH <sub>4</sub> Uptake [wt%]	H <sub>2</sub> Uptake [wt%]	Ref.
				273 K	298 K	273 K	77 K	
<i>df</i> -TzCTF600	1720	1505	0.75	6.79	4.60	4.38	2.50	Current work
HAT-CTF 450/600	1090	ND	ND	6.3	-	-	-	23
HAT-CTF-600	899	ND	ND	5.1	-	-	-	
F-DCBP-CTF-1	2437	ND	0.51	5.98	3.82	-	1.77	57
F-DCBP-CTF-2	2036	ND	0.34	5.23	3.16	-	-	
CTF-py	1239	ND	0.45	5.08	3.79	-	1.63	95
<i>bipy</i> -CTF500	1548	ND	ND	5.34	3.07	-	1.63	56
<i>lut</i> -CTF500	1680	ND	ND	5.04	2.58	-	1.60	
FCTF-1-600	1535	752	ND	5.53	3.41	ND	ND	55

ND: not determined

## Section T. Supporting References:

### References:

S1:	H. H. Wenk and W. Sander, <i>Eur. J. Org. Chem.</i> , 2002, <b>23</b> , 3927-3935.
S2:	Y. Tobe, N. Nakagawa, J. Kishi, M. Sonoda, K. Naemura, T. Wakabayashi, T. Shida, and Y. Achiba, <i>Tetrahedron</i> , 2001, <b>57</b> , 3629-3636.
S3:	O. K. Farha, A. Ö. Yazaydın, I. Eryazıcı, C. D. Malliakas, B. G. Hauser, M. G. Kanatzidis, S. T. Nguyen, R. Q. Snurr and J. T. Hupp, <i>Nature Chemistry</i> , 2010, <b>2</b> , 944-948.

S4:	Y. -L. Zhao, L. Liu, W. Zhang, C. -H. Sue, Q. Li, O. Š. Miljanić, O. M. Yaghi and J. F. Stoddart, <i>Chem. Eur. J.</i> , 2009, <b>15</b> , 13356-13380.
S5:	K. V. Kutonova, M. E. Trusova, P. S. Postnikov, V. D. Filimonov and J. Parello <i>Synthesis</i> , 2013, <b>45</b> , 2706-2710.
S6:	M. Matti Maricq and J. S. Waugh, <i>J. Chem. Phys.</i> , 1979, <b>70</b> , 3300-3316.
S7:	H. Wu, K. Yao, Y. Zhu, B. Li, Z. Shi, R. Krishna and J. Li, <i>J. Phys. Chem. C</i> , <b>2012</b> , <i>116</i> , 16609-16618.
S8:	A. L. Myers and J. M. Prausnitz, <i>A.I.Ch.E.J.</i> 1965, <b>11</b> , 121-130.
S9:	S. -Y. Yu, J. Mahmood, H. -J. Noh, J. -M. Seo, S. -M. Jung, S. -H. Shin, Y. -K. Im, I. -Y. Jeon and J. -B. Baek, <i>Angew. Chem. Int. Ed.</i> , 2018, <b>57</b> , 8438-8442.
S10:	S. Ren , M. J. Bojdys , R. Dawson , A. Laybourn , Y. Z. Khimiyak , D. J. Adams and A. I. Cooper, <i>Adv. Mater.</i> , 2012, <b>24</b> , 2357-2361.
S11:	P. Puthiaraj, S. -S. Kim and W. -S. Ahn, <i>Chem. Eng. J.</i> , 2016, <b>283</b> , 184-192.
S12:	L. Tao, F. Niub, C. Wanga, J. Liuc, T. Wanga and Q. Wang, <i>J. Mater. Chem. A</i> , 2016, <b>4</b> , 11812-11820.
S13:	P. Puthiaraj, S. -M. Cho, Y.-R. Lee and W. -S. Ahn, <i>J. Mater. Chem. A</i> , 2015, <b>3</b> , 6792-6797.
S14:	S. Dey, A. Bhunia, D. Esquivel and C. Janiak, <i>J. Mater. Chem. A</i> , 2016, <b>4</b> , 6259-6263.
S15:	T. Wang, Y.-C. Zhao, L.-M. Zhang, Y. Cui, C.-S. Zhang and B. -H. Han, <i>Beilstein J. Org. Chem.</i> , 2017, <b>13</b> , 2131-2137.
S16:	S. Bandyopadhyay, A. G. Anil, A. James and A. Patra, <i>ACS Appl. Mater. Interfaces</i> , 2016, <b>8</b> , 27669-27678.
S17:	T. Islamoglu, S. Behera, Z. Kahveci, T.-D. Tessema, P. Jena and H. M. El-Kaderi, <i>ACS Appl. Mater. Interfaces</i> , 2016, <b>8</b> , 14648-14655.
S18:	MD. W. Hussain, S. Bandyopadhyay and A. Patra, <i>Chem. Commun.</i> , 2017, <b>53</b> , 10576-10579.
S19:	M. G. Rabbani, T. E. Reich, R.M. Kassab, K. T. Jackson and H. M. El-Kaderi, <i>Chem. Commun.</i> , 2012, <b>48</b> , 1141-1143.
S20:	P. Arab, M. G. Rabbani, A. K. Sekizkardes, T. İslamoğlu and H. M. El-Kaderi, <i>Chem. Mater.</i> , 2014, <b>26</b> , 1385-1392.
S21:	X. Zhang, J. Lu and J. Zhang, <i>Chem. Mater.</i> , 2014, <b>26</b> , 4023-4029.
S22:	M. G. Rabbani and H. M. El-Kaderi, <i>Chem. Mater.</i> , 2012, <b>24</b> , 1511-1517.
S23:	A. K. Sekizkardes, T. Islamoğlu, Z. Kahveci and H. M. El-Kaderi, <i>J. Mater. Chem. A</i> , 2014, <b>2</b> , 12492-12500.
S24:	S. Mondal and N. Das, <i>J. Mater. Chem. A</i> , 2015, <b>3</b> , 23577-23586.
S25:	Y. Yuan, P. Cui, Y. Tian, X. Zou, Y. Zhou, F. Sunb and G. Zhu, <i>Chem. Sci.</i> , 2016, <b>7</b> , 3751-3756.
S26:	C. Pei, T. Ben, Y. Li and S. Qiu, <i>Chem. Commun.</i> , 2014, <b>50</b> , 6134-6136.
S27:	X. -J. Wang, P. -Z. Li, Y. Chen, Q. Zhang, H. Zhang, X. X. Chan, R. Ganguly, Y. Li, J. Jiang and Y. Zhao, <i>Scientific Report</i> , 2013, <b>3</b> , 1149
S28:	J. M. Roberts, B. M. Fini, A. A. Sarjeant, O. K. Farha, J.T. Hupp and K. A. Scheidt, <i>J. Am. Chem. Soc.</i> , 2012, <b>134</b> , 3334.
S29:	R. Luebke, Ł. J. Weseliński, Y. Belmabkhout, Z. Chen, Ł. Wojtas and M. Eddaoudi, <i>Cryst. Growth Des.</i> , 2014, <b>14</b> , 414.